Biosensors and Bioelectronics 124–125 (2019) 59–65

Contents lists available at ScienceDirect

Biosensors and Bioelectronics

journal homepage: www.elsevier.com/locate/bios

Electrochemiluminescence resonance energy transfer biosensor between the glucose functionalized MnO_2 and g-C_3N_4 nanocomposites for ultrasensitive detection of concanavalin A

Haifeng Sha, Yao Zhang, Yinfang Wang, Hong Ke, Xin Xiong, Nengqin Jia*

The Education Ministry Key Laboratory of Resource Chemistry, Shanghai Key Laboratory of Rare Earth Functional Materials, Department of Chemistry, Shanghai Normal University, Shanghai 200234, PR China

ARTICLE INFO

Keywords:
Electrochemiluminescence
Resonance energy transfer
Concanavalin A
G-C_3N_4-COOH@Glu
BSA@MnO_2-MWCNTs-COOH@Glu

ABSTRACT

An electrochemiluminescence (ECL) analytical platform was initially proposed based on the electrochemiluminescence resonance energy transfer (ECL-RET) mechanism for ultrasensitive detection of Concanavalin A (Con A). In this protocol, the glucose functionalized carboxylic g-C_3N_4 nanosheets (g-C_3N_4-COOH@Glu) and MnO_2 nanoparticles covered carboxylic multi-wall carbon nanotubes (BSA@MnO_2-MWCNTs-COOH@Glu) were synthesized and acted as ECL-RET electron donor and acceptor, respectively. Herein, glucose was served as the recognition element for binding Con A and MWCNTs was utilized as the carrier materials for loading MnO_2. When the quenching probe BSA@MnO_2-MWCNTs-COOH@Glu was incubated onto the modified electrodes via the specific carbohydrate-Con A interaction, the ECL signals of g-C_3N_4-COOH@Glu which used $S_2O_8^{2-}$ as its coreactant have drastically declined. Under optimum conditions, this biosensor performed a sensitive detection of the Con A ranging from 1×10^{-5} to 1×10^{4} ng/mL with a detection limit of 2.2 fg/mL (S/N = 3). Moreover, favorable analytical outcomes for detecion Con A in actual serum samples were obtained, exhibiting huge applications in clinical diagnosis of this assay.

1. Introduction

As one of the legume proteins, Concanavalin A can be collected from jack bean (Fan et al., 2016). In neutral environments, each Concanavalin A includes four recognition sites, one of which belongs to the specific recognition between Con A and carbohydrate ligands (Pu et al., 2010; Sandoval-Altamirano et al., 2017). Based on the specific recognition, Con A was selected as a protein model to study cell surface recognition, cell communication and cancer cell detection, etc (Li et al., 2017; Ou et al., 2015). So far, a number of approaches were reported for detection of Con A, containing resonance Rayleigh scattering (Yan et al., 2014), differential pulse voltammetry (Hu et al., 2012), electrochemistry analysis (Liu et al., 2014), surface plasmon resonance (Huang et al., 2013) and fluorescence spectroscopy (Chen et al., 2011), etc. Although these analytical approaches could detect the Con A, they also have several disadvantages, such as complicated instrument and equipment, long analysis time and narrow detection range.

Electrochemiluminescence (ECL) has attracted numerous researchers' interest as a result of its remarkable advantages including high sensitivity, good selectivity, strong stability, reliable accuracy and speedy assay (Muzyka, 2014; Zhang et al., 2017a). In recent years, resonance energy transfer (RET) mechanism has been frequently used in the ECL for constructing sensitive sensors (Dong et al., 2014; Ke et al., 2018). Numerous nanomaterials, such as carbon materials and transition metal oxides, have been widely utilized in fabrication of sensors owing to their excellent merits (Chen et al., 2018a, 2018b; Wang et al., 2017). For example, Zhang's group constructed an ECL immunosensor for detection AFP which utilized multi-walled carbon nanotubes as the carriers material to load more platinum nanoparticles and luminescent reagents (Zhang et al., 2017b). Liu's group prepared MnO_2 nanosheets as the base materials for ECL detection of glutathione (Gao et al., 2016). Wang's group prepared graphite-like carbon nitride nanosheets (g-C_3N_4 NSs) which used $K_2S_2O_8$ as its coreactant for ECL analysis (Wang et al., 2016).

In this work, an ultrasensitive ECL-RET sandwich biosensor was originally prepared to detect Con A via the specific carbohydrate-Con A interaction. Here, no antibody or aptamer has been used in assembly processes of biosensors, drastically improving the stability of the constructed sensor. When the quenching proble BSA@MnO_2-MWCNTs-COOH@Glu was connected to the modified electrode, the ECL intensity

* Corresponding author.
E-mail address: nqjia@shnu.edu.cn (N. Jia).

https://doi.org/10.1016/j.bios.2018.10.023
Received 29 July 2018; Received in revised form 10 October 2018; Accepted 11 October 2018
Available online 12 October 2018
0956-5663/

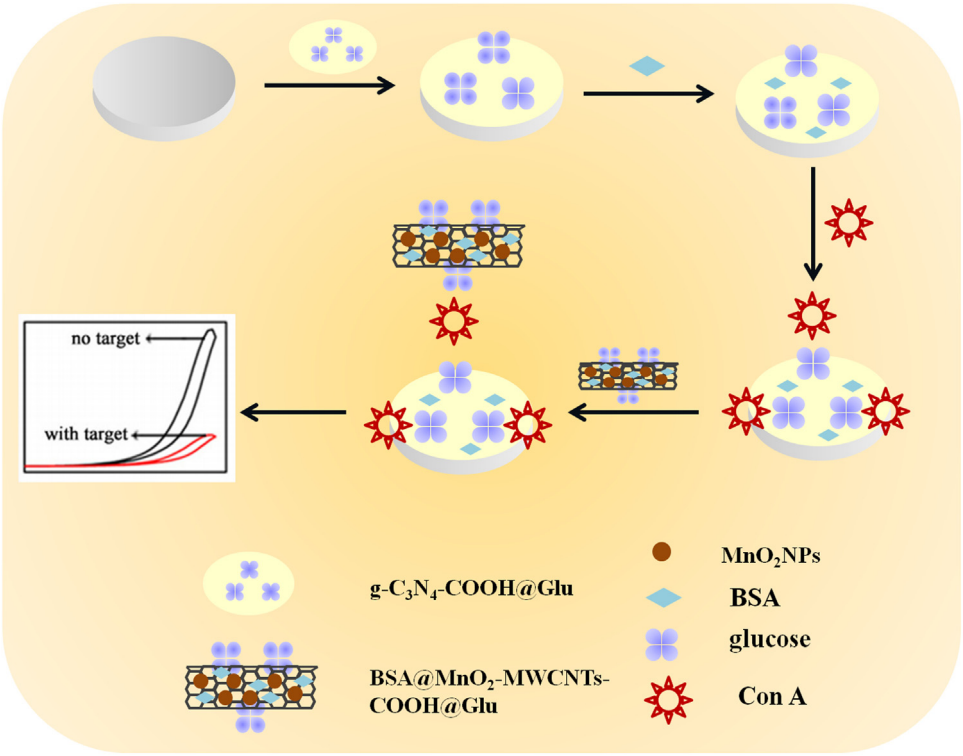

Scheme 1. The assembly process of the designed sandwich ECL-RET biosensor.

has descended obviously as a result of the quenching effect from RET between g-C_3N_4-COOH@Glu and BSA@MnO_2-MWCNTs-COOH@Glu acted as RET donor and acceptor, respectively. Based on the signal changes, the Con A could be measured sensitively and accurately. Furthermore, the designed sensor also obtained favorable analytical outcomes for determining Con A in actual serum samples, exhibiting huge applications in clinical diagnosis of this assay.

2. Experimental sections

2.1. Reagents and materials

MWCNTs were bought from Shenzhen Nanotech Port Co., (China). Melamine (99%) was gained by Energy Chemical Co., Ltd. (China). Glucose, $KMnO_4$ and $Mn(NO_3)_2$ were obtained through Sinopharm Chemical Reagent Co., Ltd, (China). N, N′-Carbonyldiimidazole (CDI) has been gained via Macklin Reagent Co., Ltd, (China). $K_2S_2O_8$ was provided through Shanghai chemical reagents Co., Ltd, (China). Concanavalin A (Con A) and bovine serum albumin (BSA, 99%) were acquired by Sigma-Aldrich Co., Ltd, (China). The human serum was supplied from Ruijin Hospital and saved at −20 °C.

2.2. Experimental instruments

Electrochemical impedance spectroscopy (EIS) and cyclic voltammetry (CV) were tested by a CHI 760B electrochemical workstation (Shanghai CH Apparatus Inc, China). The different morphologies of materials were obtained via using the Scanning electron microscopy (SEM, LEO1530 field emission, Germany). UV–vis absorption spectra were obtained by a Thermo Multiskan spectrum spectrophotometer. The resulting composites were investigated using Fourier transform infrared (FT-IR) and thermogravimetric analysis (TGA, Perkin-Elmer Pyris Diamond). ECL mesurements were carried out by MPI-E ECL analyzer (Xi'an Remax Electronic High-Tech Ltd.). Besides, a traditional three electrode system was utilized throughout ECL experimentations, including a differently decorated glassy carbon electrode (working electrode), a Pt wire (counter electrode) and Ag/AgCl (reference electrode).

2.3. Synthesis process of g-C_3N_4-COOH@Glu composite

The bulk C_3N_4 was prepared in accordance with the reported methods with some modifications (Mallakpour and Zadehnazari, 2013; Zhang et al., 2014). Firstly, 5 g of melamine was added into a alumina crucible with a lid and then heated at 600 °C for 4 h with a heating rate of 5 °C min^{-1}, ultimately producing the yellow powder. Afterwards, 1 g of bulk g-C_3N_4 was placed in mixed acid (VH_2SO_4:$VHNO_3$ = 3:1), sonicating for 12 h to get the g-C_3N_4-COOH nanosheets. Then, 50 mg g-C_3N_4-COOH nanosheets were dispersed in 10 mL CDI (10 mg/mL) solution for sonicating 1 h and then oscillation overnight under ambient condition. Next, 80 mg glucose was put into the mixture for reaction 12 h. Finally, the product was centrifuged with water and dried 12 h under 35 °C.

2.4. Synthesis of BSA@MnO_2-MWCNTs-COOH@Glu composite

Initially, the preparation of the MWCNTs-COOH was according to above-mentioned mixed acid-treated method. Subsequently, 50 mg MWCNTs-COOH and 20 mL $Mn(NO_3)_2$ (0.25 mmol) were added into 10 mL redistilled water for sonicating 30 min. Then, 10 mL $KMnO_4$ (2 mmol) was put into the mixed solution for stirring 1 h at 85 °C. Afterwards, the centrifuged deposit was dispersed into 10 mL CDI (10 mg/mL) for sonicating 1 h, oscillating overnight in ambient temperature. After that, 80 mg glucose was put into mix solution and reacted overnight at ambient temperature. After thoroughly centrifuging, the product was placed in 5 mL BSA (5 mg/mL) solution for oscillation 4 h to block nonspecific binding site. Ultimately, products were collected after centrifuging and washing.

2.5. Construction of the biosensor

Originally, the GCE was polished by 0.3 and 0.05 μm alumina

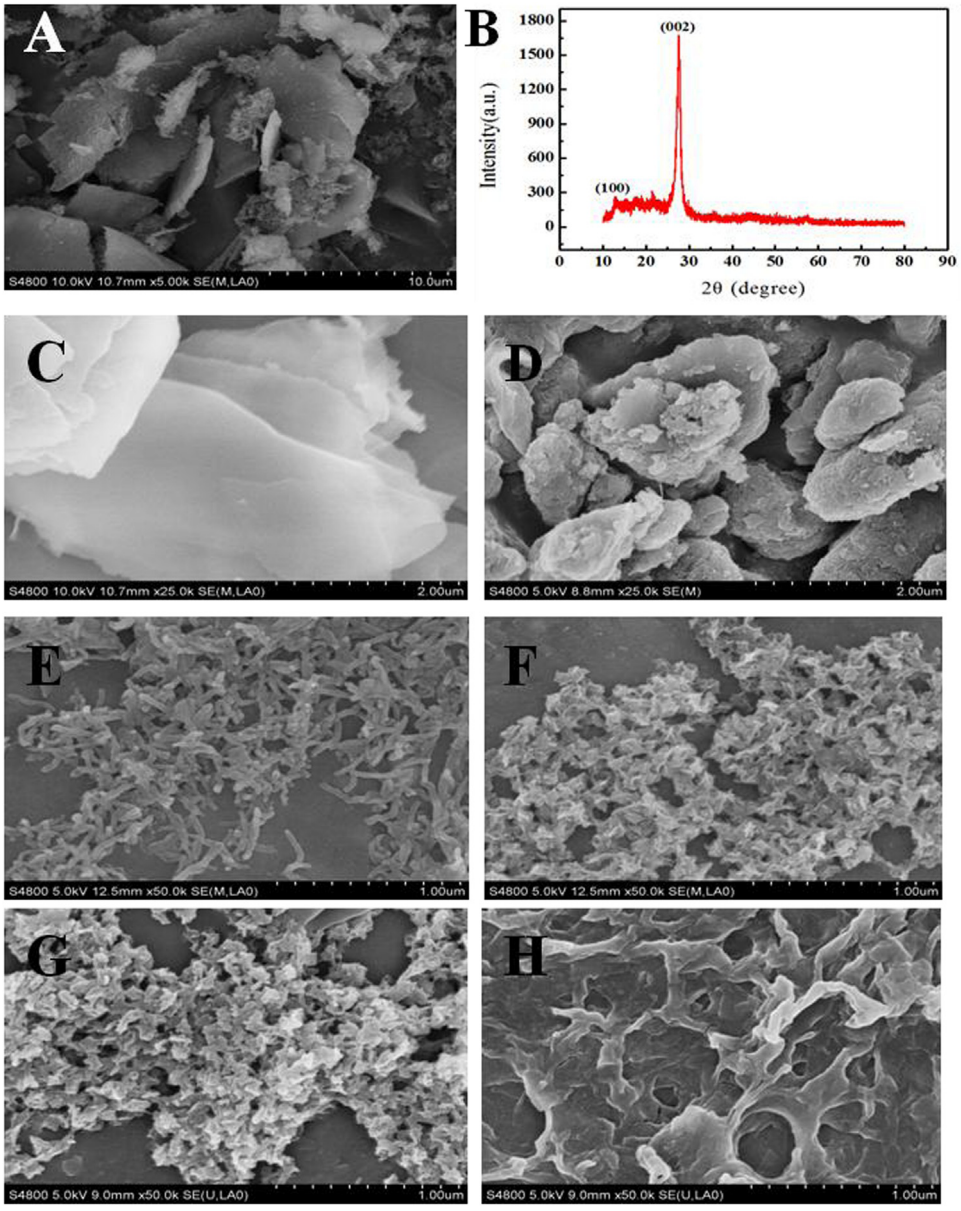

Fig. 1. SEM images of bulk g-C_3N_4 (A), g-C_3N_4-COOH (C), g-C_3N_4-COOH@Glu (D), MWCNTs-COOH (E), MnO_2-MWCNTs-COOH (F), MnO_2-MWCNTs-COOH@Glu (G) and BSA@MnO_2-MWCNTs-COOH@Glu (H). (B) XRD of bulk g-C_3N_4.

powder sequentially, cleaned by double distilled water. After that, electrodes were sonicated for 3 min in water and dried by nitrogen stream. Afterwards, 3 μL of g-C_3N_4-COOH@Glu solution was coated onto electrodes and dried in ambient temperature. Subsequently, 3 μL BSA (0.5%) was covered on GCE with 30 min for blocking non-specific binding site. After carefully rinsing by phosphate buffer (PBS), the surface-modified GCE was linked with various contents of Con A by a carbohydrate-ConA recognition reaction for 45 min in 4 °C. After that, 3 μL BSA@MnO_2-MWCNTs-COOH@Glu solution was added at the modified GCE by the carbohydrate-ConA interaction for 45 min at 4 °C. The acquired ECL biosensor was kept for the further use. Scheme 1 displayed the assembly process of the biosensor.

3. Results and discussion

3.1. Characterization of materials

The morphological of materials was characterized using FMSEM. The prepared bulk g-C_3N_4 is thick lamellar structure as depicted in Fig. 1A. Accordingly, its XRD pattern (Fig. 1B) shows two diffraction peaks at 13.12 and 27.58 degrees correspond to 100 and 002 planes, respectively, which is consistent with the previous literature (Tian et al., 2013), suggesting that the bulk g-C_3N_4 is successfully obtained. After acidizing treatment, as can be seen from Fig. 1C, the surface of g-C_3N_4-COOH is much smoother than the bulk g-C_3N_4 (Fig. 1A). After the g-C_3N_4-COOH is functionalized by glucose, its surface is covered with a layer of material, demonstrating the successful preparation of g-C_3N_4-COOH@Glu (Fig. 1D). On the other hand, the MWCNTs-COOH exhibits a regular tubular structure (Fig. 1E). As exhibited in Fig. 1F, MnO_2 nanoparticles are uniformly decorated on the MWCNTs-COOH. When glucose functionalized the MnO_2-MWCNTs-COOH, its surface is more rough (Fig. 1H). As indicated in Fig. 1G, the MnO_2-MWCNTs-COOH@Glu is coated by BSA completely, suggesting the successful synthesis of the BSA@MnO_2-MWCNTs-COOH@Glu. Furthermore, UV–Vis absorption spectras has been used to illustrate the effective loading of MnO_2 on the MWCNTs-COOH. As presented in Fig. S1, a new wide absorption peak of MnO_2 (curve b) from 250 nm to 550 nm (Gao et al., 2016) is obviously observed from the MnO_2-MWCNTs-COOH

(curve b) in contrast with the MWCNTs-COOH (curve a). When glucose (curve c) and BSA (curve d) are modified onto the MnO_2-MWCNT-COOH, the absorption peak remains unchanged, affirming the formation of MnO_2 on the MWCNTs-COOH. To further illustrate glucose is attached to the C_3N_4-COOH and MnO_2-MWCNT-COOH, the FT-IR spectra of the glucose, g-C_3N_4-COOH, g-C_3N_4-COOH@Glu, MWCNT-COOH and MnO_2-MWCNT-COOH@Glu are showed in Fig. S3. The FT-IR spectra of g-C_3N_4-COOH and g-C_3N_4-COOH@Glu are basically the same. Because the peak in the range of 1040–1114 cm^{-1} belongs to the –C–NH–C or –C–O– bonds. But there exists a new peak in this range from the MWCNT-COOH@Glu compared with the MWCNTs-COOH assigned to –C–O– bonds of glucose, suggesting that glucose was really linked to the MWCNTs-COOH. For the sake of verifying modifications of glucose on the C_3N_4-COOH and MWCNTs-COOH, thermogravimetric analysis (TGA) and differential thermal analysis (DTA) for the samples tested in a nitrogen atmosphere. As indicated in Fig S4, an initial weight loss is observed below 200 °C, which may arise from the evaporation of adsorbed water to the sample surface. A slow weight loss step occurs in the temperature range of 200–500 °C, which may be attributed to the combustion of carboxyl groups on the surface of g-C_3N_4-COOH and MWCNTs-COOH. In details, a sharp weight loss step occurs in the temperature range of 500–650 °C, which may be attributed to the thermal decomposition of the g-C_3N_4 to form graphite and N_2 (Fig S4A, curve a). The TGA of g-C_3N_4-COOH@Glu (Fig S4B, curve a) is basically the same as g-C_3N_4-COOH (Fig S4A, curve a). However, the g-C_3N_4-COOH@Glu completely decomposes at 700 °C compared with 650 °C of the g-C_3N_4-COOH as a result of the decomposition of glucose attached to the surface of g-C_3N_4-COOH, which is consistent with the TGA of glucose (Fig S4E, curve a). Furthermore, the DTA of g-C_3N_4-COOH (Fig S4A, curve b) indicates that its thermal decomposition is an exothermic reaction. But the DTA of g-C_3N_4-COOH@Glu from 600 °C to 700 °C shows an endothermic reaction (Fig S4B, curve b) due to the decomposition of glucose, which is also consistent with the DTA of glucose (Fig S4E, curve b). As indicated in Fig S4C, the weight loss of MWCNTs-COOH@Glu (curve a) has obviously declined by 54% from 200 °C to 800 °C compared with 38% of the MWCNTs-COOH (Fig S4D, curve a) owing to the presence of glucose.

3.2. Detection mechanism of the ECL biosensor

A new ECL sensor was proposed to sensitively detect Con A according to the ECL-RET mechanism between glucose functionalized g-C_3N_4 and MnO_2 nanocomposites. As seen in Fig. 2A, the UV–vis absorption (curve a) and ECL spectrum emission (curve b) spectra of the g-C_3N_4-COOH@Glu exhibit an absorption peak and an ECL emission peak occurs at 296 nm and 440 nm respectively (Wang et al., 2016). As depicted in Fig. 2B, the wide absorption of BSA@MnO_2-MWCNTs-COOH@Glu (curve a) can quench the ECL emission at 440 nm of g-C_3N_4-COOH@Glu (curve b) due to the large overlap between the ECL emission spectrum of donor (g-C_3N_4) and the UV–Vis absorption spectrum of acceptor (MnO_2). $K_2S_2O_8$ is often applied to increase the ECL intensity of g-C_3N_4 as its coreactant. The specific luminescence mechanism between g-C_3N_4 and $S_2O_8^{2-}$ may as follows:

$$g\text{-}C_3N_4 + e^- \rightarrow g\text{-}C_3N_4^{\bullet -} \quad (1)$$

$$S_2O_8^{2-} + e^- \rightarrow SO_4^{2-} + SO_4^{\bullet -} \quad (2)$$

$$g\text{-}C_3N_4^{\bullet -} + SO_4^{\bullet -} \rightarrow g\text{-}C_3N_4^{*} + g\text{-}C_3N_4 \quad (3)$$

$$g\text{-}C_3N_4^{*} \rightarrow g\text{-}C_3N_4 + h\nu \quad (4)$$

3.3. Electrochemical and Electrochemiluminescence behaviors of the biosensor

To explore the conductivity of the carrier material MWCNTs, cyclic voltammetry was used in this work. As displayed in Fig. S2, the current intensity of MWCNTs-COOH modified GCE (curve b) is evidently higher than that of the bare GCE (curve a), illustrating the superior conductivity of the MWCNTs-COOH. For the sake of investigating interface performances of electrodes during assembly process, the electrochemical impedance spectroscopy is a powerful way. According to Fig. 3A, it shows the electronic transfer resistance (Ret) of each modified step. Comparing g-C_3N_4-COOH@Glu modified electrodes (curve b) with bare electrodes (curve a), the resistance becomes a little bigger due to the poor conductivity of glucose. The resistance values significantly increase after the electrode was successively connected with BSA (curve c) and ConA (curve d), which are attributed to the hindrance effect of interfacial electron transfer from the proteins. When the GCE was linked to the BSA@MnO_2-MWCNTs-COOH@Glu (curve e), the Ret values improve obviously owing to the presence of nonconductive materials (glucose and BSA) impeding the electron transfer. The results illustrate the successful assemble of the ECL biosensor.

As exhibited in Fig. 3B, the electrochemiluminescence behavior of each assembly process was also studied. ECL signals of g-C_3N_4-COOH@Glu modified GCE have increased greatly in 0.1 M PBS buffer (pH = 7.4) with 0.25 M $K_2S_2O_8$ solution (curve b) compared to absence of $K_2S_2O_8$ (curve a). It shows that $K_2S_2O_8$ can dramatically improve the luminescence of g-C_3N_4. The ECL responses have continuously decreased after BSA (curve c) and Con A (curve d) were successively dropped onto the modified GCE because proteins impeded the electron transfer. After the quenching probe BSA@MnO_2-MWCNTs-COOH@Glu (curve e) was linked to the electrodes, the ECL signal has a significant drop owing to the ECL-RET reaction between the RET acceptor MnO_2 and donor g-C_3N_4.

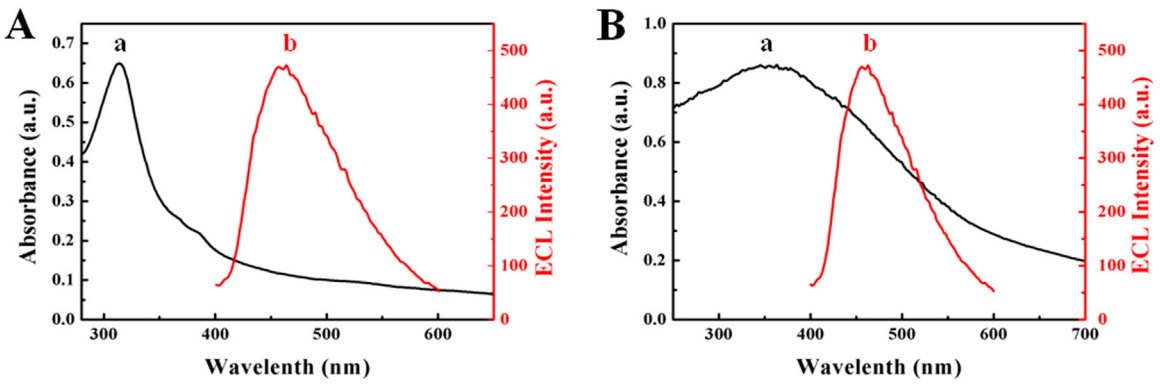

Fig. 2. (A) UV–vis absorption spectra (a) and ECL spectrum (b) of g-C_3N_4-COOH@Glu. (B) UV–vis absorption spectra of BSA@MnO_2-MWCNTs-COOH@Glu (a) and ECL spectrum of g-C_3N_4-COOH@Glu (b).

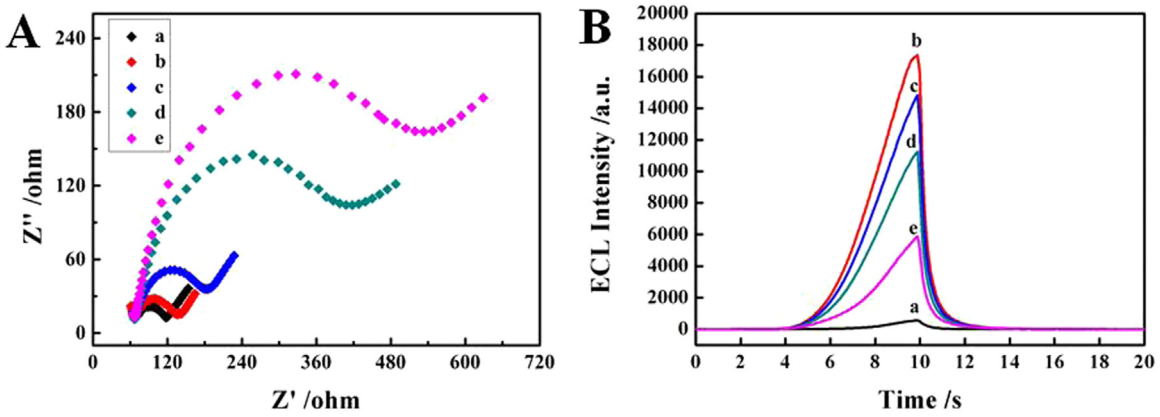

Fig. 3. (A) Impedance plots of the assemble process at different modified electrodes: (a) bare GCE, (b) g-C_3N_4-COOH@Glu/GCE, (c) BSA/g-C_3N_4-COOH@Glu/GCE, (d) Con A/BSA/g-C_3N_4-COOH@Glu/GCE, (e) BSA@MnO_2-MWCNTs-COOH@Glu/Con A/BSA/C_3N_4-COOH@Glu/GCE in 0.1 M KCl containing 5 mM $Fe(CN)_6^{3-/4-}$. (B) ECL responses of g-C_3N_4-COOH@Glu/GCE in 0.1 M PBS (pH 7.4) without (a) and with 0.025 M $K_2S_2O_8$ (b), and (c) BSA/g-C_3N_4-COOH@Glu/GCE, (d) Con A/BSA/g-C_3N_4-COOH@Glu/GCE, (e) BSA@MnO_2-MWCNTs-COOH@Glu/Con A/BSA/C_3N_4-COOH@Glu/GCE in 0.1 M PBS (pH 7.4) with 0.025 M $K_2S_2O_8$.

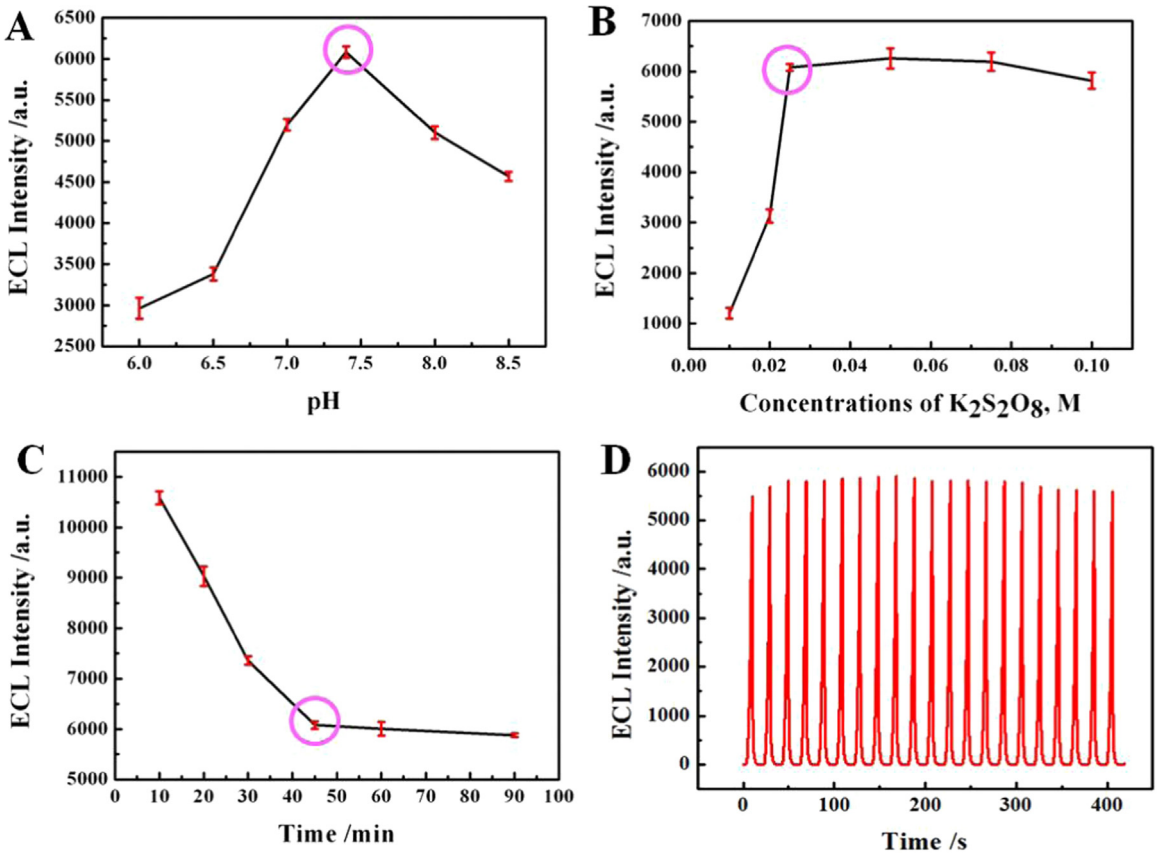

Fig. 4. Influences of (A) pH, (B) binding time between Con A and glucose and (C) concentration of $K_2S_2O_8$. (D) The ECL signal-time curve of 0.1 ng/mL Con A in 0.1 M PBS (pH 7.4) with 0.025 M $K_2S_2O_8$ from − 2.0–0 V for 21 cycles with the scan rate of 100 mV s^{-1}.

3.4. Optimization of experimental conditions

Some influencing parameters, such as pH, content of $K_2S_2O_8$ and binding time between the Con A and glucose, have been studied in this work. As indicated in Fig. 4A, the pH of PBS buffer range from 6.0 to 8.5 is investigated, and the strongest luminescent signal appears at 7.4 because high or low pH will have an adverse impact on the immobilized process of protein. Thus, near-neutral pH (7.4) is selected as the optimal pH. As the concentration of $K_2S_2O_8$ is constantly rising from 0.01 M to 0.1 M, the ECL signal reaches the maximum at 0.025 M and it remains basically unchanged when the concentration continues to increase (Fig. 4B). So 0.025 M of $K_2S_2O_8$ is used for the following experiments. Afterwards, the effect of binding time between the Con A and glucose is shown in Fig. 4C. As the binding time increases to 45 min, the ECL intensity approaches to the minimum and it achieves plateau when the time continues to mount up. Consequently, 45 min is used for following studies. It can be seen from Fig. 4D that the ECL signal is extremely stable in optimized conditions.

3.5. Detection of Con A via the ECL biosensor

Under the optimal condition, the designed ECL biosensor has been

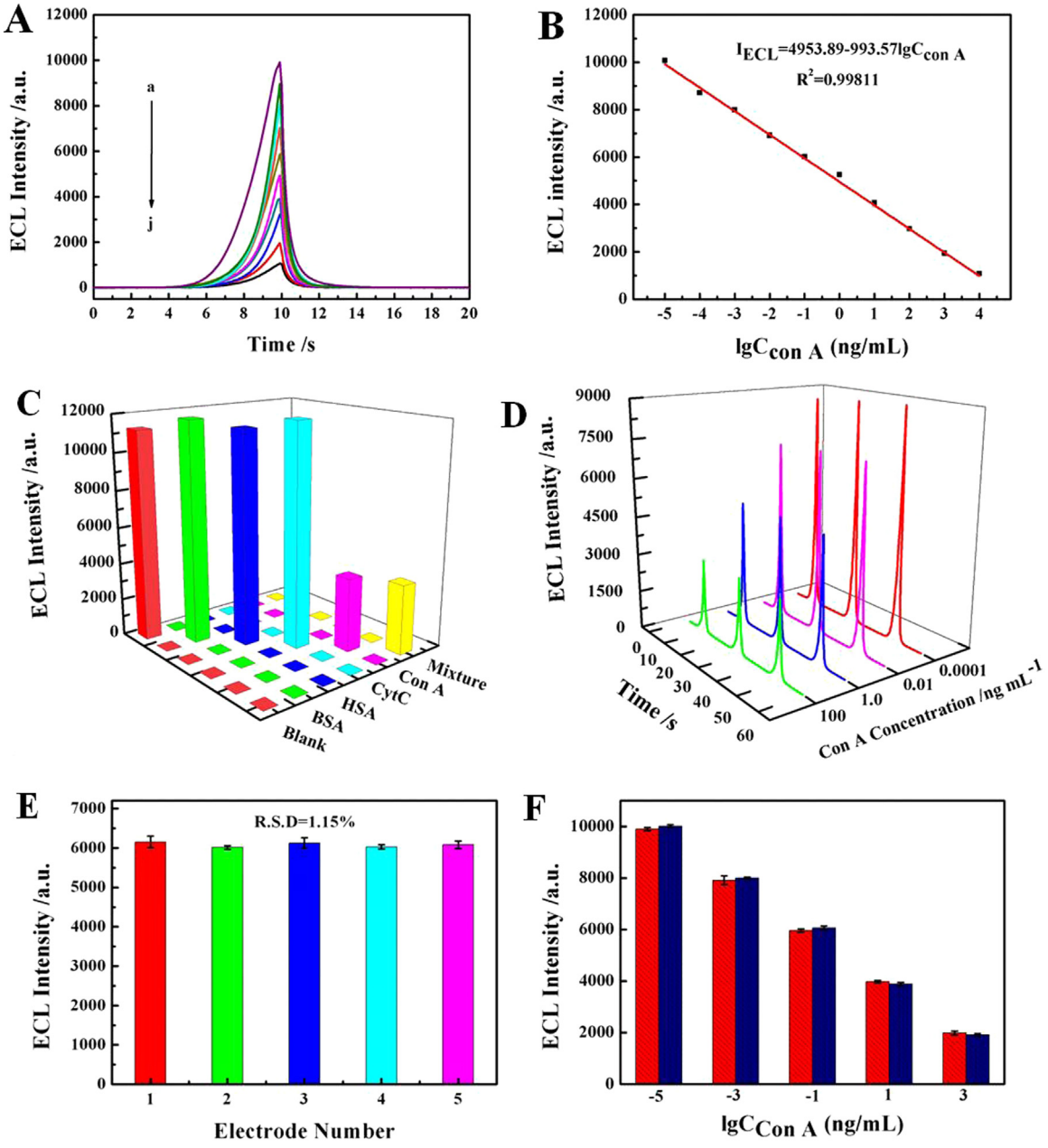

Fig. 5. (A) Electrochemiluminescence signals for Con A detection with the prepared sensor. Con A concentrations (ng/mL): (a) 0.00001, (b) 0.0001, (c) 0.001, (d) 0.01, (e) 0.1, (f) 1, (g) 10, (h) 100, (i) 1000 and (j) 10,000. (B) Calibration curve of the ECL biosensor. (C) The specificity of the constructed ECL immunsensor: blank, BSA (0.1 mg/mL), HSA (0.1 mg/mL), CytC (0.1 mg/mL), Con A (10 ng/mL) and mixture (10 ng/mL Con A with 0.1 mg/mL interferences). (D) The stability of the proposed ECL sensor with different Con A concentration. (E) Reproducibility of the prepared sensor with five electrodes (0.1 ng/mL Con A). (F) Comparison of ECL intensity of different AFP concentrations and different conditions (the red one is Con A in the PBS, and the blue one is Con A in the diluted serum).

applied in ultrasensitive detection of Con A. As exhibited from Fig. 5A, luminescence signals gradually decline (curve a-j) accompanying the increase contents of Con A. Accordingly, the calibration curve with good linear correlation (Fig. 5B) is acquired between ECL intensities and logarithms of Con A concentration ranging from 1.0×10^{-5} to 1.0×10^{4} ng/mL with the low detection limit (LOD) of 2.2 fg/mL. The linear regression equation is $I_{ECL} = 4953.89–993.57lgC_{Con\ A}$ with the correlation coefficient (R^2) of 0.9981. Furthermore, the comparison between this work and previous works illustrates that the prepared biosensor has a wider linear detection range and a lower LOD (Table S1).

3.6. Selectivity, stability and repeatability of sensors

The selectivity, stability and reproducibility of this prepared biosensor have been explored under optimal conditions. As shown in Fig. 5C, when 0.1 mg/mL of BSA, human serum albumin (HAS) and cytochrome C (Cyt C) are used to replace Con A, the ECL intensity has no obvious decline like the blank (no Con A). However, the luminous intensity of the sensors rapidly decreases after the Con A (0.1 ng/mL) or the mixture is added. The test indicates that the constructed sensor has excellent selectivity for detecting the Con A. Fig. 5D displays that the ECL signals with different Con A concentration has the good stability to detect the Con A. The repeatability of the sensor is depicted in Fig. 5E by comparing the ECL signals of the five same electrodes. The ECL intensity remains almost unchanged with R.S.D of 1.15%, suggesting the

preeminent repeatability of this sensor.

Moreover, the histogram (Fig. 5F) clarifies the potential application at diverse experimental conditions (red columns and blue columns represent the PBS and diluted human serum separately) via the comparison of ECL intensities. The experimental results suggest that the ECL signals in different environments are basically the same, indicating the satisfied detection of Con A in actual clinical samples.

3.7. Analysis of actual samples

The application in real serum sample of the prepared ECL biosensor was studied with a standard addition method. Table S2 illustrates that the recovery rates of the Con A (95.35–105.44%) and its corresponding RSDs (0.67–3.71%) are satisfactory within a reasonable error range, further suggesting that the constructed ECL-RET biosensor is a feasible and reliable method to detect Con A in actual human serum.

4. Conclusion

To summarize, a new ECL-RET biosensor has been assembled for ultrasensitive detection of Con A. After the BSA@MnO_2-MWCNTs-COOH@Glu connected to the GCE due to the specific carbohydrate-Con A interaction, the ECL signals of g-C_3N_4-COOH@Glu have declined evidently. The possible quenching mechanism between the MnO_2 and g-C_3N_4 may be ascribed to the ECL-RET. Furthermore, the prepared biosensor displayed good selectivity, favorable stability and repeatability, showing its great application prospect in real clinical analysis.

Acknowledgments

We are grateful for financial support from the Shanghai Science and Technology Committee (17070503000, 18dz2308700), National Natural Science Foundation of China (21373138) Program for Changjiang Scholars and Innovative Research Team in University (IRT_16R49) and International Joint Laboratory on Resource Chemistry (IJLRC).

Appendix A. Supplementary material

Supplementary data associated with this article can be found in the online version at doi:10.1016/j.bios.2018.10.023.

References

Chen, Q., Wei, W., Lin, J.M., 2011. Homogeneous detection of concanavalin A using pyrene-conjugated maltose assembled graphene based on fluorescence resonance energy transfer. Biosens. Bioelectron. 26 (11), 4497–4502.
Chen, Y.X., Huang, K.J., He, L.L., Wang, Y.H., 2018a. Tetrahedral DNA probe coupling with hybridization chain reaction for competitive thrombin aptasensor. Biosens. Bioelectron. 100, 274–281.
Chen, Y.X., Huang, K.J., Niu, K.X., 2018b. Recent advances in signal amplification strategy based on oligonucleotide and nanomaterials for microRNA detection-a review. Biosens. Bioelectron. 99, 612–624.
Dong, Y.P., Gao, T.T., Zhou, Y., Zhu, J.J., 2014. Electrogenerated chemiluminescence resonance energy transfer between luminol and CdSe@ZnS quantum dots and its sensing application in the determination of thrombin. Anal. Chem. 86 (22), 11373–11379.
Fan, Y., Tan, X., Ou, X., Lu, Q., Chen, S., Wei, S., 2016. A novel "on-off" electrochemiluminescence sensor for the detection of concanavalin A based on Ag-doped g-C_3N_4. Electrochim. Acta 202, 90–99.
Gao, W., Liu, Z., Qi, L., Lai, J., Kitte, S.A., Xu, G., 2016. Ultrasensitive glutathione detection based on Lucigenin cathodic electrochemiluminescence in the presence of MnO_2 nanosheets. Anal. Chem. 88 (15), 7654–7659.
Hu, F., Chen, S., Wang, C., Yuan, R., Xiang, Y., Wang, C., 2012. Multi-wall carbon nanotube-polyaniline biosensor based on lectin-carbohydrate affinity for ultrasensitive detection of Con A. Biosens. Bioelectron. 34 (1), 202–207.
Huang, C.F., Yao, G.H., Liang, R.P., Qiu, J.D., 2013. Graphene oxide and dextran capped gold nanoparticles based surface plasmon resonance sensor for sensitive detection of concanavalin A. Biosens. Bioelectron. 50, 305–310.
Ke, H., Sha, H., Wang, Y., Guo, W., Zhang, X., Wang, Z., Huang, C., Jia, N., 2018. Electrochemiluminescence resonance energy transfer system between GNRs and Ru $(bpy)_3(^{2+})$: application in magnetic aptasensor for beta-amyloid. Biosens. Bioelectron. 100, 266–273.
Li, X., Wang, Y., Shi, L., Ma, H., Zhang, Y., Du, B., Wu, D., Wei, Q., 2017. A novel ECL biosensor for the detection of concanavalin A based on glucose functionalized $NiCo_2S_4$ nanoparticles-grown on carboxylic graphene as quenching probe. Biosens. Bioelectron. 96, 113–120.
Liu, B., Zhang, B., Chen, G., Yang, H., Tang, D., 2014. Proximity ligation assay with three-way junction-induced rolling circle amplification for ultrasensitive electronic monitoring of concanavalin A. Anal. Chem. 86 (15), 7773–7781.
Mallakpour, S., Zadehnazari, A., 2013. One-pot synthesis of glucose functionalized multi-walled carbon nanotubes: dispersion in hydroxylated poly(amide-imide) composites and their thermo-mechanical properties. Polymer 54 (23), 6329–6338.
Muzyka, K., 2014. Current trends in the development of the electrochemiluminescent immunosensors. Biosens. Bioelectron. 54, 393–407.
Ou, X., Tan, X., Liu, X., Lu, Q., Chen, S., Wei, S., 2015. A signal-on electrochemiluminescence biosensor for detecting Con A using phenoxy dextran-graphite-like carbon nitride as signal probe. Biosens. Bioelectron. 70, 89–97.
Pu, K.-Y., Shi, J., Wang, L., Cai, L., Wang, G., Liu, B., 2010. Mannose-substituted conjugated polyelectrolyte and oligomer as an intelligent energy transfer pair for label-free visual detection of concanavalin A. Macromolecules 43 (23), 9690–9697.
Sandoval-Altamirano, C., Sanchez, S.A., Ferreyra, N.F., Gunther, G., 2017. Understanding the interaction of concanavalin a with mannosyl glycoliposomes: a surface plasmon resonance and fluorescence study. Colloids Surf. B: Biointerfaces 158, 539–546.
Tian, J., Liu, Q., Ge, C., Xing, Z., Asiri, A.M., Al-Youbi, A.O., Sun, X., 2013. Ultrathin graphitic carbon nitride nanosheets: a low-cost, green, and highly efficient electrocatalyst toward the reduction of hydrogen peroxide and its glucose biosensing application. Nanoscale 5 (19), 8921–8924.
Wang, Y.H., Huang, K.J., Wu, X., 2017. Recent advances in transition-metal dichalcogenides based electrochemical biosensors: a review. Biosens. Bioelectron. 97, 305–316.
Wang, Y.Z., Hao, N., Feng, Q.M., Shi, H.W., Xu, J.J., Chen, H.Y., 2016. A ratiometric electrochemiluminescence detection for cancer cells using g-C_3N_4 nanosheets and Ag-PAMAM-luminol nanocomposites. Biosens. Bioelectron. 77, 76–82.
Yan, S., Zhang, L., Tang, Y., Lv, Y., 2014. Synthesis of water-soluble $Ag(_2)Se$ QDs as a novel resonance Rayleigh scattering sensor for highly sensitive and selective ConA detection. Analyst 139 (17), 4210–4215.
Zhang, X., Guo, W., Wang, Z., Ke, H., Zhao, W., Zhang, A., Huang, C., Jia, N., 2017a. A sandwich electrochemiluminescence immunosensor for highly sensitive detection of alpha fetal protein based on MoS2-PEI-Au nanocomposites and Au@BSA core/shell nanoparticles. Sens. Actuators B: Chem. 253, 470–477.
Zhang, X., Ke, H., Wang, Z., Guo, W., Zhang, A., Huang, C., Jia, N., 2017b. An ultrasensitive multi-walled carbon nanotube–platinum–luminol nanocomposite-based electrochemiluminescence immunosensor. Analyst 142 (12), 2253–2260.
Zhang, X.L., Zheng, C., Guo, S.S., Li, J., Yang, H.H., Chen, G., 2014. Turn-on fluorescence sensor for intracellular imaging of glutathione using g-$C(_3)N(_4)$ nanosheet-$MnO(_2)$ sandwich nanocomposite. Anal. Chem. 86 (7), 3426–3434.